Available online at www.sciencedirect.com

SciVerse ScienceDirect

Journal of the European Ceramic Society 32 (2012) 2909–2915

www.elsevier.com/locate/jeurceramsoc

Transparent polycrystalline alumina obtained by SPS: Green bodies processing effect

Lucile Lallemant [a,b,*], Gilbert Fantozzi [a,b], Vincent Garnier [a,b], Guillaume Bonnefont [a,b]

[a] *Université de Lyon, CNRS, France*
[b] *Insa-Lyon, MATEIS UMR5510, F-69621 Villeurbanne, France*

Available online 18 March 2012

Abstract

Starting from a commercial slurry of high purity α-Al_2O_3, freeze-dried powders, cast, filter-pressed or cold isostatically pressed samples were produced. Resulting powders or green bodies showing different particles packing were densified by spark plasma sintering (SPS) to obtain transparent polycrystalline α-Al_2O_3. Microstructure and real in-line transmittance (RIT) after SPS were dependent on the particles packing quality. Avoiding large agglomerates, narrowing the pore size distribution, reducing the most-frequent pore size (D_{mode}) and avoiding macroscopic heterogeneities within the green bodies enabled high RIT values to be achieved in the visible and near-infrared spectrum. However, a limit was achieved in the preparation of green bodies for which reducing the D_{mode} had no more influence on the optical behaviour of samples sintered by SPS. Finally, pure α-Al_2O_3 samples presenting a high $RIT_{640\,nm}$ value of 53% were produced from all the green bodies obtained by the following techniques: filter-pressing, slip casting and cold isostatic pressing.

Keywords: Al_2O_3; Shaping; Porosity; Spark plasma sintering; Optical properties

1. Introduction

Obtaining transparent polycrystalline ceramics became an important technological challenge over the last decade.[1–14] Their high mechanical properties combined with a high transparency and a reasonable price could lead to the replacement of glasses or sapphire monocrystals in optical applications (windows, armours, discharge lamps envelopes, and jewellery). Nevertheless, to obtain high light transmission, the microstructure has to be carefully controlled and all the sources of light scattering have to be avoided (inclusions, second phases, porosity). Pure polycrystalline alumina (PCA) possesses mechanical properties (hardness, fracture toughness, flexural strength) among the highest for oxide compounds explaining why PCA is one of the most studied materials regarding these applications. However, because of PCA's birefringent nature, a good transparency is more difficult to obtain than for cubic materials. Indeed, light is not only scattered by porosity but also by grain boundaries. The real in-line transmittance (RIT) of PCA is generally characterised by a model developed by Apetz and van Bruggen[1] based on the Rayleigh–Gans–Debye approximation but other models have been developed. Pecharroman et al.[2] suggested characterising grain boundary scattering as a function of a textural angle, which corresponds to the grain orientation organisation of the ceramic. As the two models are equivalent for a textural angle of 41°, which is not too far from a random orientation (45°), it was decided to compare our own results with Apetz's model (Eqs. (1) and (2)).

$$\mathrm{RIT} = \frac{I_2}{I_1} = (1 - R_S)\exp(-\gamma_{tot} D) \tag{1}$$

$$\gamma_{tot} = \gamma_G + \gamma_p = \frac{3\pi^2 r \Delta n^2}{{\lambda_0}^2} = \frac{p}{(4/3)\pi \cdot r_p^3} \cdot C_{sca,p} \tag{2}$$

with I_1 and I_2 the light beam intensities before and after travelling through a sample having a thickness D; R_s the total normal surface reflectance (=0.14 for PCA); γ_{tot} the total scattering coefficient; γ_G the light scattering coefficient by grain boundaries; γ_p the light scattering coefficient by porosities; r the average grain radius; Δn the average refractive index change between two adjacent grains (=0.005 for PCA), λ_0 the wavelength of incident light beam in vacuum; p the total porosity, r_p the average pore radius and $C_{sca,p}$ the scattering cross section of

* Corresponding author at: Insa-Lyon, MATEIS UMR5510, F-69621 Villeurbanne, France.
E-mail address: lucile.lallemant@insa-lyon.fr (L. Lallemant).

0955-2219/$ – see front matter © 2012 Elsevier Ltd. All rights reserved.
doi:10.1016/j.jeurceramsoc.2012.02.041

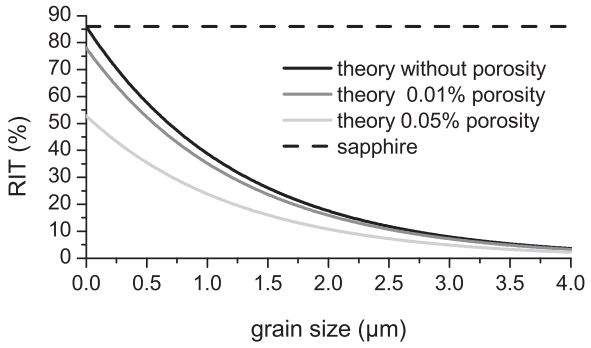

Fig. 1. Influence of grain size and porosity (pore diameter 100 nm – λ = 640 nm) according to the optical model (Eq. (1)) on the RIT of PCA.

one spherical pore. In Figs. 1 and 2, showing respectively, the RIT of PCA as a function of grain size and porosity size, it can be seen that to obtain a high value of RIT, PCA should possess after sintering, grains as small as possible and a porosity closed to 0.00% with the smallest pores possible. To obtain such kind of microstructure, different strategies can be used from the composition of the starting powder to the sintering technique. The use of doping elements (Mg, Y, La, Zr. . .) has been shown to reduce grain size and recently Stuer et al.[3] and Roussel et al.[4] succeeded in improving the RIT of PCA at values close to 50% at 640 nm for a sample thickness of 0.88 mm by adding doping elements to the powder (respectively, 54.7% by tri-doping the powder with Mg, Y and La and 48.1% by doping the powder with La). In both cases, the spark plasma sintering technique was used as it gives fully dense ceramics at low temperature for short hold times, allowing to maintain a small grain size. Nevertheless, this technique requires a careful control of sintering parameters.[15] Kim et al.[5,6] have shown that for low applied pressure (below 80 MPa which is the highest pressure supported by the graphite die), the heating rate has to be low in order to remove the last few pores. They were able to obtain a RIT of 47% on a pure alumina sample after sintering with a heating rate of 8 °C/min. By increasing the applied pressure up to 500 MPa, Grasso et al.[7] produced a highly transparent pure alumina sample (64% at 645 nm) at low temperature (around 1000 °C). As this high pressure cannot be achieved with regular graphite die, a specific WC matrix had been designed for this experiment. Nevertheless, in all the previously mentioned studies, the powder was directly put into the

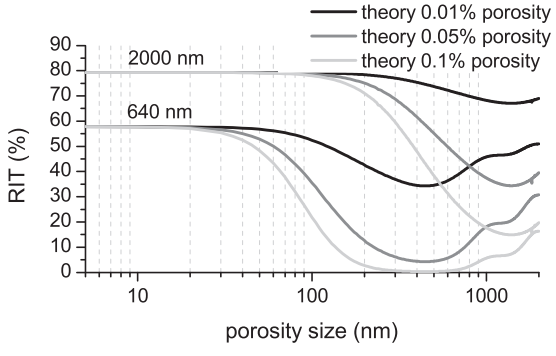

Fig. 2. Influence of porosity size and porosity (grain size 500 nm – λ = 640–2000 nm) according to the optical model (Eq. (1)) on the RIT of PCA.

die without improving the processing technique. However, it is well known that this step can significantly help the densification step. Some authors[8–10,13,16–18] have shown that narrowing pore size distribution and reducing pore size in the green compact gives an increase of the green body's density leading to samples with high sintered densities at lower temperatures with minimal grain growth. By using respectively filter pressing or slip casting method, Petit et al.[8] and Krell et al.[9] were able to improve the transparency of PCA naturally sintered and HIPed (hot isostatic pressing) up to 72% for Krell et al. Aman et al.[10] recently studied the influence of green shaping on spark plasma sintered PCA. The used sintering cycle prevented them from obtaining transparent samples but they showed that samples with homogeneous green compacts and small most-frequent pore size (D_{mode}) can favour densification and lead to higher sintered density also with SPS technique. In the present study, we will combine the beneficial effects of controlled green shaping and spark plasma sintering to obtain pure transparent PCA with regular graphite die (i.e. at low pressure).

2. Material and methods

The starting material was a commercial (BA15psh, Baïkowski) high purity α-Al_2O_3 aqueous slurry (solid content 73.5 wt.%) with a median particle size D_{50}^{v} of 150 nm (measured by laser diffraction). The total impurity amount was less than 0.01 wt.% (14 ppm Na, 60 ppm K, 7.1 ppm Fe, 13 ppm Si, 4 ppm Ca) as reported by the manufacturer.

Four different processing techniques were used to obtain well dispersed powder or green bodies from the commercial slurry (pH 3.5 without any additives):

(1) Freeze-drying (FD samples): the slurry was frozen in liquid nitrogen and freeze-dried for approximately 48 h (−40 °C, 0.1 mbar, Alpha2-4, Christ) to obtain a powder. The powder was then sieved at 500 μm.
(2) Slip casting of two different slurries. The slip casting ability of the slurries was measured by determining the stress threshold (τ_H) (Viscotester VT500/501, Haake, Karlsruhe, Germany). (C1 samples): the slurry (τ_H = 1.18 Pa) was directly cast onto 20 mm diameter porous alumina moulds in order to avoid contamination of the green bodies by impurity diffusion. After 4 h, the samples were removed from the moulds and put in a desiccator for 24 h. (C2 samples): a second batch of the BA15psh slurry, more difficult to cast than the first one because of a higher shear stress (τ_H = 3.48 Pa), was also slip cast.
(3) Slip casting followed by cold isostatic pressing (CIP samples): cold isostatic pressing was performed on C1 cast samples under a pressure of 3600bars (ACB, Nantes, France).
(4) Filter pressing (FP samples): The slurry was directly cast onto a polyester filter (pore diameter = 0.2 μm). After pushing the liquid across the filter using a pressure of 35 bar, green bodies were removed from the 20 mm diameter mould and dried at 70 °C for 12 h.

All the green bodies were then manually polished to obtain 2 g cylindrical samples. Pore size distributions in green bodies were determined by mercury infiltration (Autopore III, Micromeritics Instrument Corp., Norcross, GA). The highest pressure reached by this apparatus is 414 MPa, which enables a minimum pore entrance diameter of 3 nm. Considering cylindrical pores of diameter d and a pressure (P) of intruded mercury, the Laplace–Washburn equation gives a $d = A/P$ relationship with A a constant containing the contact angle between the alumina and the mercury. A 130° angle was used in our calculations.

Densification of FD powder and C1, C2, CIP and FP green bodies was carried out by SPS (HP D 25/1, FCT Systeme, Rauenstein, Germany) using the following sintering cycle: applied uniaxial pressure of 80 MPa throughout the cycle, rapid heating up to 800 °C, heating rate of 10 °C/min from 800 °C to 1100 °C followed by a slower heating (1 °C/min) up to the final sintering temperature (T_f) in order to remove the residual porosity.[4–6,19] The final sintering temperature was in the 1130–1230 °C range and was optimised for each green body's processing route. A rapid cooling ended the cycle, interrupted by a 10 min dwell at 1000 °C to release the residual stresses.[4–6] Then, the samples were carefully mirror-polished on both sides using diamond slurries (to 1 μm) and the transparency in the centre of the pellet (spot size = 5 mm × 2 mm) was evaluated by a real in-line transmittance (RIT) measurement (Jasco V-670), because it only takes into account the unscattered light through the sample (i.e. the real transmitted light) as explained by Apetz and van Bruggen.[1] All the RIT values given in this paper are evaluated for λ = 640 nm and Eq. (3) is used to obtain the RIT at the same thickness of $t_2 = 0.88$ mm in order to be able to compare the results:

$$\mathrm{RIT}(t_2) = (1 - R_S)\left(\frac{\mathrm{RIT}(t_1)}{1 - R_S}\right)^{t_2/t_1} \quad (3)$$

where R_S is the total normal surface reflectance (=0.14 for PCA) and RIT (t_i) is the RIT for a sample thickness t_i.

SEM ZEISS Supra55 was used to investigate the microstructure of the samples. Grain sizes were evaluated on thermally etched surfaces (at a temperature 50 °C lower than T_f for 1 h and a heating rate of 10 °C/min) and a factor of 1.56 was applied to obtain a revised grain size[21] using the intercept method.

3. Results and discussion

3.1. Green body's characterisation

The commercial high purity α-alumina slurry was either freeze-dried and uniaxially pressed (50 MPa) or colloidally formed by different techniques (slip casting, slip casting followed by CIP or filter pressing) to obtain green bodies with different degrees of particle packing. Geometrical bulk density measurements were performed and compared to the theoretical density (TD) of alumina (3.987 g cm^{-3}). Green densities were evaluated on several samples for each green body's processing route to ensure reproducibility. They show an increase of density from FD pressed samples to CIP samples (52%TD for FD samples, 54%TD for FP and C2 samples, 56%TD for C1 samples and 58%TD for CIP samples). C2 samples present a lower bulk density compared to C1 samples, which can be explained by its viscous behaviour: agglomeration of particles had probably occurred leading to a less dense particles packing. The porosity distribution was evaluated by mercury infiltration on several samples for each green body and a very good reproducibility was observed. Fig. 3 displays the *absolute* pore distributions in which a decrease of the pore volume is observed as expected from the geometrical bulk densities evaluated above (from FD pressed samples presenting the highest pore volume and therefore the lowest bulk density to CIP samples presenting the lowest pore volume and consequently the highest bulk density). In order to compare microstructures with different total absolute pore volume, Fig. 4 provides the *relative* pore volume distributions[10,16] whereas Fig. 5 displays the incremental pore volume distributions. All Figs. 3–5 tend to show that FD pressed samples present a larger pore size distribution as porosities in the 50 nm − 1 μm range are present. These porosities are attributed to large residual inter-granular porosities from the freeze-dried powder that the pressing step was not able to remove. They give evidence of the presence of large agglomerates formed during the drying step.[4] Other samples present finer pore size distributions but a closer look on small porosities (<100 nm) is necessary to evaluate the difference between the samples (Fig. 5). Samples prepared with the same slurry (i.e. FP, C1 and CIP samples) present a similar pore distribution with a steep slope at the centre of the distribution (Fig. 4). The main difference is the D_{mode} which decreases from FP samples to CIP samples – 40 nm for FP samples, 32 nm for C1 samples and 25 nm for CIP samples, respectively (Fig. 5). These results are in good agreement with some authors[10,20] who

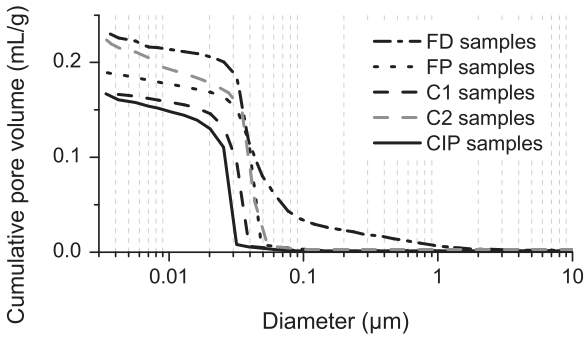

Fig. 3. Absolute cumulative pore size distributions of each investigated microstructures.

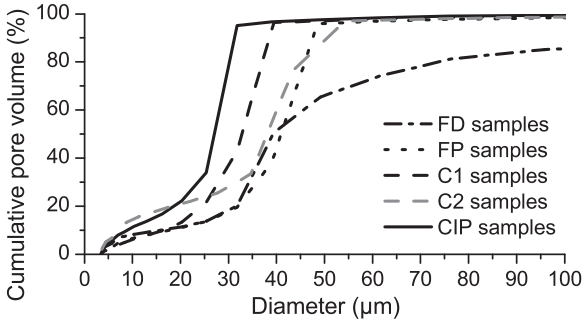

Fig. 4. Relative cumulative pore size distributions of each investigated microstructures (total porosity is taken as a parameter).

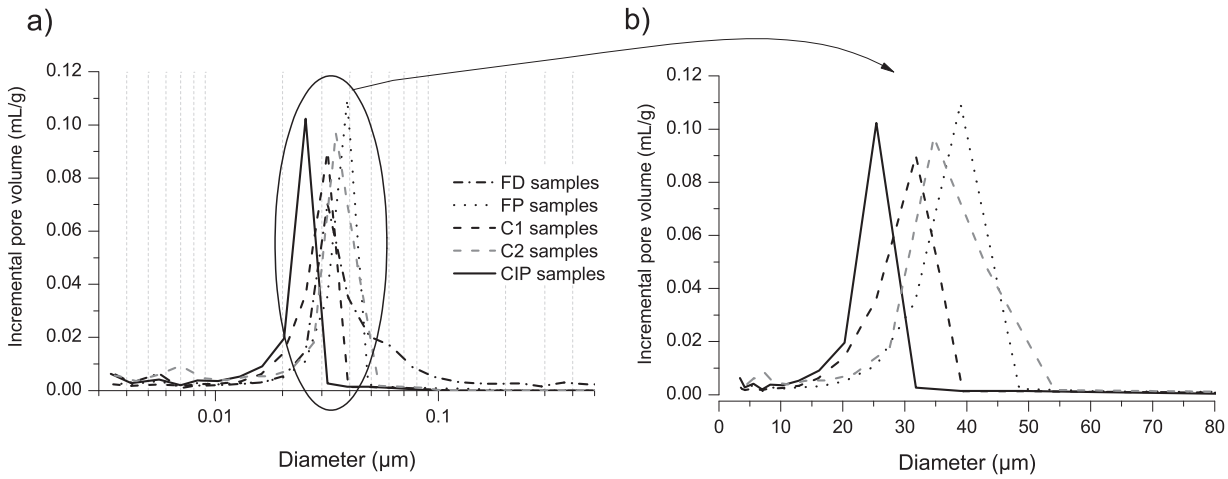

Fig. 5. Incremental pore size distribution of each investigated microstructures: (a) [0–0.5 μm] diameter range, and (b) [0–80 nm] diameter range without FD samples.

found a relationship between the D_{mode} and the green compacts densities: the finer the D_{mode} is, the higher the green density is. C2 samples present a main pore size close to 35 nm, which is not so far from the one of C1 samples (32 nm). Nevertheless, the distribution of pore is larger (10–55 nm) than the other samples – respectively (20–48 nm) for FP samples, (14–40 nm) for C1 samples and (10–32 nm) for CIP samples (Fig. 5) and the slope at the centre of the distribution is gentler (Fig. 4). Complementary porosity distribution measurements were performed on C1 and C2 20 mm diameter samples to compare the centre and the edges of the samples. If the porosity distribution is the same all over the C1 sample, the edges of the C2 sample present more larger pores than the centre (Fig. 6) resulting in a macroscopic more heterogeneous particle packing. All these differences (larger pore distribution with higher amount of smaller pores, gentler slope at the centre of the pore distribution, macroscopic heterogeneous distribution of pore within the sample) are attributed to drying issues in samples cast from the most viscous slurry.

Finally, we were able to prepare samples with different particles packing:

(A) Pressed samples (FD) of a freeze-dried powder present the lowest green body's density, a larger pore size distribution with large porosities coming from large agglomerates.

(B) Cast samples from a viscous slurry (C2) present a larger pore size distribution compared to other wet-processed samples and a heterogeneous macroscopic particle packing within the sample.

(C) Three wet-processed samples (FP, C1 and CIP) present a narrower pore size distribution and a homogeneous macroscopic particle packing but increasing green body density with decreasing D_{mode}.

3.2. Sintering behaviour and optical properties

The freeze-dried powder was put directly into the graphite die and then sintered by SPS at different final temperatures (T_f) to optimise the RIT at the centre of the pellets. Indeed, RIT of PCA is known to strongly depend on both porosity and grain size. Temperature is then a key parameter as a too low temperature will leave porosity while a too high temperature will induce grain growth.[4] In the present study, an increase of grain size is noticed from 0.52 ± 0.11 μm at 1180 °C to 1.93 ± 0.35 μm at 1280 °C. RIT measurements of samples sintered at different T_f were performed on visible and near IR spectrum (300–2500 nm) and are presented in Fig. 7. For T_f above 1230 °C, a decrease of RIT is observed all over the spectrum when increasing the temperature. This decrease is attributed to grain growth (Fig. 1). Samples sintered at T_f below 1230 °C present equivalent or

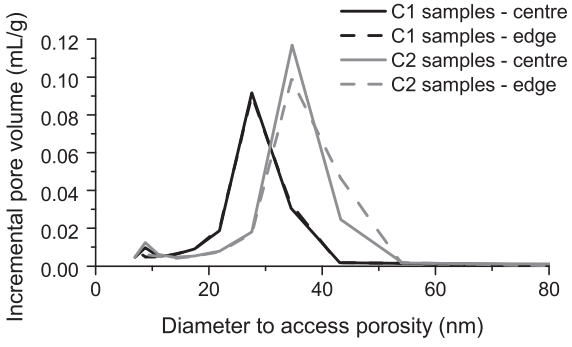

Fig. 6. Comparison of the incremental pore size distribution on the centre and the edges of cast samples (C1 and C2).

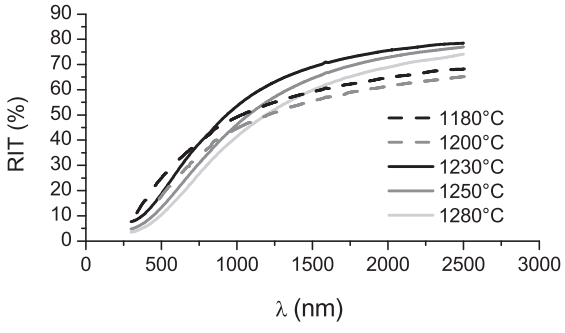

Fig. 7. RIT measurements on 300–2500 nm wavelength range of pure freeze-dried alumina powders sintered by SPS at different T_f.

Table 1
Samples characteristics after sintering at an optimised T_f.

Sample	Optimised T_f (°C)	$RIT_{640\,nm}$ (%)	Average grain size after SPS (μm)
FD powder	1230	30.5	1.17 ± 0.20
FP samples	1130	52.0	0.48 ± 0.15
C1 samples	1130	53.1	0.44 ± 0.09
C2 samples	1150	45.6	0.48 ± 0.13
CIP samples	1130	52.9	0.43 ± 0.12

even higher RIT values in the visible range compared to the other samples. However, RIT values are clearly inferior in the IR wavelengths. It can be explained by large pores, which are more critical on optical properties in the IR wavelengths than in the visible range (Fig. 2). Densification is not optimum below 1230 °C, which is consequently the preferred T_f to sinter FD powders by SPS in this study. As all the densities are up to 99.9%, the Archimedes's method is not precise enough to support these measurements.

Wet-processed green body's pellets (FP, C1, C2 and CIP) were also sintered at different T_f to optimise the RIT. Higher $RIT_{640\,nm}$ values were obtained at a lower optimised T_f (around 100 °C) compared to the freeze-dried powder (see Table 1). At higher temperatures, wet-processed samples become less transparent due to grain growth (1.85 ± 0.44 μm for C1 samples sintered at 1230 °C).

The freeze-dried powder contains some large agglomerates (see Section 3.1) formed during the drying step. According to Lange,[22] during conventional sintering, shrinkage will begin within these agglomerates, increasing the size and coordination number of the inter-agglomerate pores. Those pores will be more stable and shrink at higher temperature leading to grain growth. This differential shrinkage occurs during SPS sintering of the freeze-dried powder explaining the higher optimised T_f. The resulting grain size (around 2.5 times higher than for other samples) explains the low RIT all over the visible and near IR spectrum (Fig. 8). The wet-processed samples have all a similar grain size around 0.45 μm after sintering due to a lower T_f. Aman et al.[19] and Santanach et al.[23] also obtained densification without grain growth at low temperature (<1200 °C). However, C2 samples present a lower $RIT_{640\,nm}$ value at slightly higher temperature compared to the other samples. FP, C1 and CIP samples present a similar microstructure with small pores

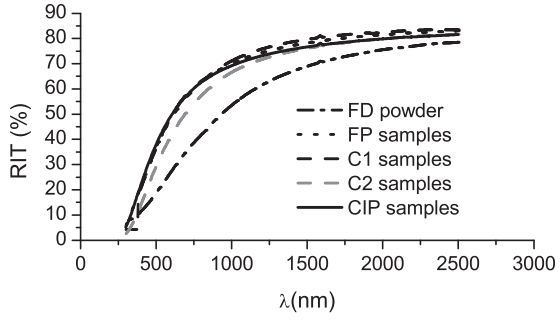

Fig. 8. RIT measurements on 300–2500 nm wavelength range of pure alumina processed by different shaping techniques and sintered by SPS at optimised T_f.

(<50 nm) whereas 100 nm size pores are found on C2 samples (Fig. 9). If these large porosities are critical in the visible range and can explain the lower $RIT_{640\,nm}$ value of C2 samples, they have nearly no influence on the IR wavelengths explaining the same behaviour of all the wet-processed samples (including C2) in the near IR wavelengths (Fig. 2). The macroscopic heterogeneous particle packing of C2 green samples probably leads to differential shrinkage between the centre and the edges of the samples, explaining the higher T_f and the microstructure differences. Some authors (Roosen and Bowen,[20] Krell et al.[13,16] and Aman et al.[10]) have demonstrated that if a small D_{mode} within the green body (i.e. high green body density) is necessary to achieve high density at lower temperatures for both natural or SPS sintering, the homogeneity within this green compact is also a key point. A narrow pore size distribution with small pores will impede the onset of grain growth during the intermediate stage of SPS sintering[10] and favour densification by grain sliding and rearrangement explaining the high sintered density at lower temperature. To obtain transparency, the last hundredth of a percent of porosity have to be eliminated and HIP is generally used after natural sintering.[8–9,11–13,16–17] In our study, the very low heating rate (1 °C/min) ending the cycle enables to achieve transparency by delaying the pore/boundary separation at high sintered temperatures.[19] Nevertheless, C2 samples probably get lower density all over the cycle due to the macroscopic heterogeneity of this particle packing and especially at 1100 °C, just before starting the low heating rate of 1 °C/min. From this lower density and because of the presence of larger pores, those are not eliminated at the end of the cycle even at a higher T_f.

The homogeneous wet-processed green bodies (FP, C1 and CIP) present different D_{mode} (see Section 3.1) but have similar optical behaviours after sintering at the same T_f (Fig. 8). According to literature for natural sintering on spinel followed by HIP,[17] we would expect to get higher transparency for the green sample presenting the narrowest pore size distribution with the lowest D_{mode}. In the present study, a limit seems to be reached for which decreasing the D_{mode} in the green body will also tend to a limit of the optical properties even if the green body is macroscopically homogeneous. This difference of behaviour between this study and the literature can be linked either to the starting slurry quality (particle size and morphology, particle surfaces) or to the sintering technique. Indeed spinel is not a birefringent material, which means that an increase of RIT is linked to a decrease in the pore size and/or amount. The higher pressure (200 MPa) and the fact that this pressure is isostatic by HIP help to close the finest pores that the small pressure of 80 MPa used in the present study cannot close. This is consistent with Grasso's study[7] which shows that a high $RIT_{645\,nm}$ value of 64% could be obtained on PCA by increasing the SPS pressure up to 500 MPa.Furthermore, this pressure also enables to sinter at a lower temperature and therefore to limit the grain growth. Finally, the same best $RIT_{640\,nm}$ value of 53% is reached for all the prepared samples whatever the preparation technique provided that those samples present a macroscopic homogeneous particles packing with a D_{mode} inferior to 40 nm (Fig. 10).

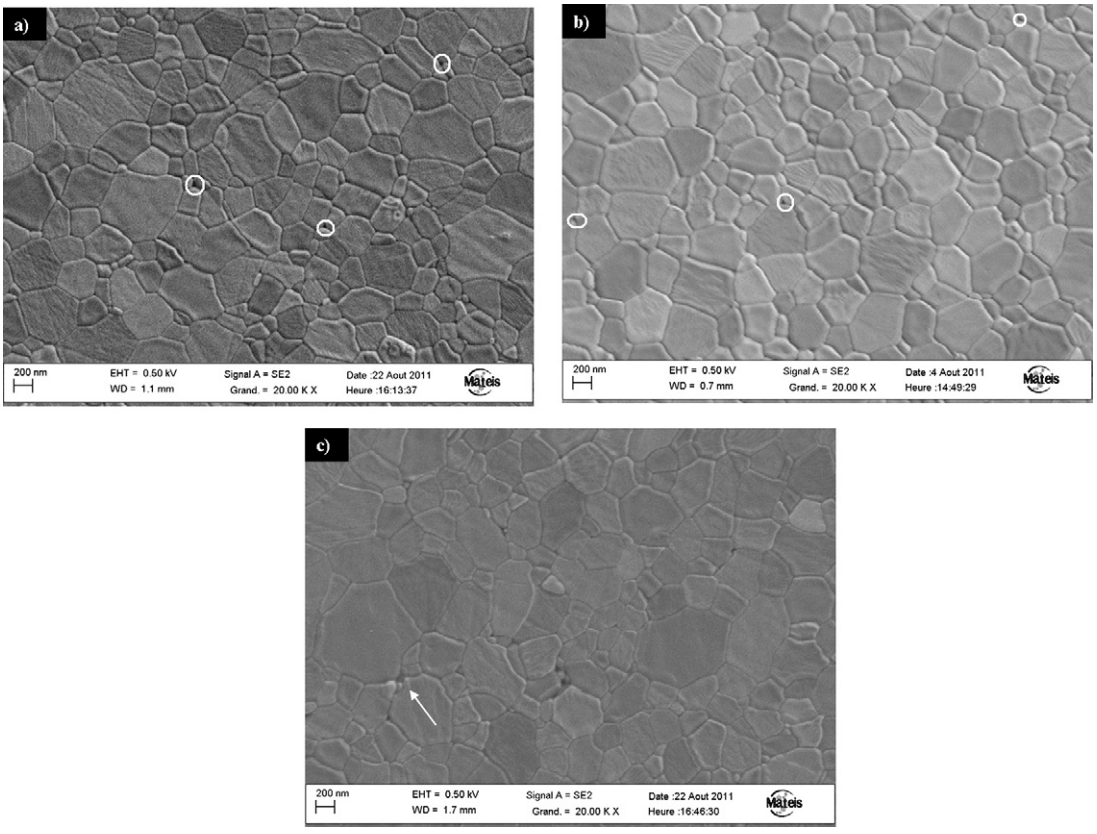

Fig. 9. SEM pictures (20,000×) of pure alumina processed by different shaping techniques and sintered by SPS at optimised T_f: (a) FP samples, (b) C1 samples, and (c) C2 samples.

Fig. 10. 20 mm diameter FP sample sintered by SPS at $T_f = 1130\,^{\circ}C$ (th = 1.4 mm – $RIT_{640\,nm} = 52.0\%$ – average grain size = $0.48 \pm 0.15\,\mu m$).

4. Conclusions

Obtaining transparent PCA requires a careful control of the green body's processing:

(1) Large agglomerates have to be avoided because they lead to differential shrinkage. Stable pores shrinking at high temperature will be created and grain growth will occur decreasing the RIT values in the visible and near-IR spectrum.
(2) Particle's packing has to be as homogeneous as possible in term of pore size (narrowest distribution). Moreover, this particle's packing has also to be macroscopically homogeneous to prevent differential shrinkage within the green body. Pores possessing a critical size (∼100 nm) will then be created and the RIT value will decrease in the visible range.
(3) Green density has to be high which implies a close particle spacing (a small D_{mode}). This primary particle arrangement will need less energy to sinter as less particle rearrangement will be necessary during SPS sintering. High densities will be obtained at lower temperatures. However, a limit exists in the preparation of green bodies for which reducing the D_{mode} in a green body (fulfilling the two previous requirements) has no more influence on the optical behaviour of the sample after SPS sintering. This limit was not noticed for samples densified by natural sintering followed by HIP.

Finally, green bodies having all these characteristics (no large agglomerates, narrow pore size distribution with small D_{mode}, macroscopically homogeneous) were produced by filter-pressing, slip casting and cold isostatic pressing. They all lead to pure α-Al_2O_3 samples presenting a high $RIT_{640\,nm}$ value of 53% after densification by SPS.

Acknowledgements

This work is a part of the CeraTRANS project. We would like to thank the ANR (French National Research Agency) for its funding support. We also would like to acknowledge Nicolas Roussel from CIRIMAT (UMR CNRS 5085), Sandrine Trombert and Lionel Bonneau from Baïkowski and Emilie Tchadjinana from MATEIS (UMR CNRS 5510) for their help in the green body's preparation, respectively freeze-drying, filter pressing and slip casting.

References

1. Apetz R, van Bruggen MPB. Transparent alumina: a light-scattering model. *J Am Ceram Soc* 2003;**86**(3):480–6.
2. Pecharromann C, Mata-Osoro G, Diaz LA, Torrecillas R, Moya JS. On the transparency of nanostructured alumina: Rayleigh–Gans model for anisotropic spheres. *Opt Express* 2009;**17**:6899–912.
3. Stuer M, Zhao Z, Aschauer U, Bowen P. Transparent polycrystalline alumina using spark plasma sintering: effect of Mg, Y and La doping. *J Eur Ceram Soc* 2010;**30**(3):1335–43.
4. Roussel N, Lallemant L, Durand B, Guillemet S, Chane Ching JY, Fantozzi G, et al. Effects of the nature of the doping salt and of the thermal pre-treatment and sintering temperature on Spark Plasma Sintering of transparent alumina. *Ceram Int* 2011.
5. Kim BN, Hiraga K, Morita K, Yoshida H. Spark plasma sintering of transparent alumina. *Scripta Mater* 2007;**57**:607–10.
6. Kim BN, Hiraga K, Morita K, Yoshida H. Effects of heating rate on microstructure and transparency of spark-plasma-sintered alumina. *J Eur Ceram Soc* 2009;**29**:323–7.
7. Grasso S, Kim BN, Hu C, Maizza G, Sakka Y. Highly transparent pure alumina fabricated by high-pressure spark plasma sintering. *J Am Ceram Soc* 2010;**93**(9):2460–2.
8. Petit J, Dethare P, Sergent A, Marino R, Ritti RH, Landais S, et al. Sintering of α-alumina for highly transparent ceramic applications. *J Eur Ceram Soc* 2011;**31**(11):1957–63.
9. Krell A, Klimke J, Hutzler T. Advanced spinel and sub-μm Al_2O_3 for transparent armour applications. *J Eur Ceram Soc* 2009;**29**:275–81.
10. Aman Y, Garnier V, Djurado E. Influence of green state processes on the sintering behaviour and the subsequent optical properties of spark plasma sintered alumina. *J Eur Ceram Soc* 2009;**29**:3363–70.
11. Krell A, Hutzler T, Klimke J. Transmission physics and consequences for materials selection, manufacturing, and applications. *J Eur Ceram Soc* 2009;**29**:207–21.
12. Krell A, Klimke J, Hutzler T. Transparent compact ceramics: inherent physical issues. *Opt Mater* 2009;**31**:1144–50.
13. Krell A, Blank P, Ma H, Hutzler T, Nebelung M. Processing of high-density submicrometer Al_2O_3 for new applications. *J Am Ceram Soc* 2003;**86**(4):546–53.
14. Kim BN, Hiraga K, Morita K, Yoshida H, Miyazaki T, Kagawa Y. Microstructure and optical properties of transparent alumina. *Acta Mater* 2009;**57**:1319–26.
15. Aman Y, Garnier V, Djurado E. A screening design approach for the understanding of spark plasma sintering parameters: a case of translucent polycrystalline undoped alumina. *Int J Appl Ceram Technol* 2010;**7**(5):574–86.
16. Krell A, Klimke J. Effects of the homogeneity of particle coordination on solid-state sintering of transparent alumina. *J Am Ceram Soc* 2006;**89**(6):1985–92.
17. Krell A, Hutzler T, Klimke J, Potthoff A. Fine-grained transparent spinel windows by the processing of different nanopowders. *J Am Ceram Soc* 2010;**93**(9):2656–66.
18. Azar M, Palmero P, Lombardi M, Garnier V, Montanaro L, Fantozzi G, et al. Effect of initial particle packing on the sintering of nanostructured transition alumina. *J Eur Ceram Soc* 2008;**28**:1121–8.
19. Aman Y, Garnier V, Djurado E. Spark plasma sintering kinetics of pure α-alumina. *J Am Ceram Soc* 2011:1–9.
20. Roosen A, Bowen HK. Influence of various consolidation techniques on the green microstructure and sintering behaviour of alumina powders. *J Am Ceram Soc* 1988;**71**(11):970–7.
21. Mendelson MI. Average grain size in polycrystalline ceramics. *J Am Ceram Soc* 1969;**52**:443–6.
22. Lange FF. Sinterability of agglomerated powders. *J Am Ceram Soc* 1984;**67**(2):83–9.
23. Santanach JG, Weibel A, Estournès C, Yang Q, Laurent Ch, Peigney A. Spark plasma sintering of alumina: study of parameters, formal sintering analysis and hypotheses on the mechanism(s) involved in densification and grain growth. *Acta Mater* 2011;**59**(4):1400–8.